Ann. Geophys., 31, 359–375, 2013
www.ann-geophys.net/31/359/2013/
doi:10.5194/angeo-31-359-2013
© Author(s) 2013. CC Attribution 3.0 License.

Annales Geophysicae
Open Access

Statistical characteristics of PMWE observations by the EISCAT VHF radar

I. Strelnikova[1] **and M. Rapp**[2]

[1]Leibniz-Institute of Atmospheric Physics, Schlossstrasse 6., 18225 Kühlungsborn, Germany
[2]German Aerospace Center Institute of Atmospheric Physics, Oberpfaffenhofen, Germany

Correspondence to: I. Strelnikova (strelnikova@iap-kborn.de)

Received: 13 September 2012 – Revised: 22 December 2012 – Accepted: 31 January 2013 – Published: 28 February 2013

Abstract. In the present paper ∼ 32.5 h of EISCAT VHF PMWE observations were analyzed with focus on spectral properties like spectral width, doppler shift and spectral shape. Examples from two days of observations with weak and strong polar mesosphere winter echo (PMWE) signals are presented and discussed in detail. These examples reveal a large variability from one case to the other. That is, some features like an observed change of vertical wind direction and spectral broadening can be very prominent in one case, but unnoticeable in the other case. However, for all observations a change of spectral shape inside the layer relative to the incoherent background is noticed.

Keywords. Radio science (Remote sensing)

1 Introduction

Polar mesosphere winter echoes or PMWE are coherent VHF radar echoes which primarily occur during the winter months in the mid-mesosphere from ∼ 55–85 km altitude at both northern and southern latitudes (e.g. Czechowsky et al., 1979; Ecklund and Balsley, 1981; Collis et al., 1992; Belova et al., 2005; Zeller et al., 2006; Kirkwood, 2007; Lübken et al., 2007; Rapp et al., 2011; Morris et al., 2011). The occurrence rate of PMWE is positively correlated with the ionization level of the D-region. Previous work has clearly shown that a sufficiently high ionization level caused e.g. by sufficiently large, highly energetic proton (and electron) fluxes or enhanced X-ray fluxes are an essential prerequisite for the existence of PMWE (Kirkwood et al., 2002; Zeller et al., 2006; Kirkwood et al., 2006a).

Because PMWE are a rare phenomena (according to Zeller et al., 2006, the mean occurrence rates is 2.9 % at polar and 0.3 % at mid-latitudes for radar frequencies of ∼53.5 MHz), their main features have so far not been investigated well. In consequence, the origin of these echoes is still under debate. Initial explanations of PMWEs were related to neutral air turbulence associated with atmospheric gravity wave breaking in the mesosphere (e.g. Ecklund and Balsley, 1981; Collis et al., 1992). Later investigations confirmed this early proposal (e.g. Lübken et al., 2006, 2007; Rapp et al., 2011; Morris et al., 2011). However, measurements with lidar and radar (Kirkwood et al., 2002; Stebel et al., 2004; Belova et al., 2005; Kero et al., 2008; La Hoz and Havnes, 2008) have triggered the hypothesis that small charged aerosol particles (probably of meteoric origin) play a similar role as in the case of PMSE (e.g. Rapp and Lübken, 2004). An alternative explanation of PMWE has been proposed by Kirkwood et al. (2006b); Kirkwood (2007). These authors argue that PMSE could possibly be caused by the scatter from highly damped ion–acoustic waves generated by partial reflection of infrasonic waves. This could possibly explain observed features like very large horizontal velocities (observed by ESRAD 50 MHz MST radar) and spectral widths (observed by EISCAT VHF radar on 10 November 2004) which show no differences between the coherent PMWE and the incoherent scatter background .

Spectral width analyses of incoherent scatter (IS) radar measurements of PMWE have so far only appeared in three previous papers, namely in the studies by Kirkwood et al. (2006b), Kirkwood (2007), and Lübken et al. (2007). Notably, all those case studies focused on the same measurements conducted during one single day, i.e. on 10 November 2004. Kirkwood et al. (2006b) and Kirkwood (2007) analyzed spectral width and doppler shift and found no difference in those parameters inside and outside the PMWE layer.

Lübken et al. (2007) further analyzed the spectral shape and found Gaussian shaped spectra inside the PMWE layer and Lorentzian outside. Since no other PMWE events (observed by IS radars) has been analyzed until now, this single day example was considered as representative of IS measurements of PMWE. As we will show further below, analysis of only two successive days can lead us to different conclusions regarding spectral width and vertical wind inside and outside the PMWE layer. Namely, on 10 November 2004 spectral width and vertical wind are similar inside and outside the PMWE layer. In contrast, measurements during the next day, i.e. on 11 November 2004, show prominent spectral broadening inside the layer. In addition, the vertical wind also changes direction from $+10\,\mathrm{m\,s^{-1}}$ to $-10\,\mathrm{m\,s^{-1}}$ inside the layer. This finding motivated us to perform an extended study using all available data and consider the statistical significance of different features. In particular, we address the question of whether the spectra inside the PMWE layers are different from the spectra of the ambient IS background.

2 Experimental details

In this work we used measurements performed with the EISCAT VHF radar at Tromsø (69° N, 19° E). A detailed description of this radar is given in Baron (1986) and can also be found under http://www.eiscat.se/groups/Documentation/BasicInfo/about/specifications. In short, the EISCAT VHF radar is monostatic, uses a cylindrical paraboloid antenna, and runs at 1.5 MW peak power at a frequency of 224 MHz. The time resolution varies between 2 and 6 s depending on the chosen experiment. For the measurements shown further in Sect. 4, a height resolution of 300 m and a time resolution of 5 s were used, and only data obtained in the vertical beam direction were considered.

Mesospheric winds were obtained from the narrow-beam Saura MF radar measurements using the Doppler beam steering (DBS) technique. The Saura MF radar is a Doppler radar that runs at 3.17 MHz and is installed close to the Andøya Rocket Range as part of the ALOMAR observatory in Andenes (Singer et al., 1997, 2003, 2007).

3 Analysis technique

All considered data have been obtained with an EISCAT experiment called "arc-dlayer" which is a further development of another low-altitude modulation described in detail in Turunen et al. (2002). The primary data stored by "arc-dlayer" are autocorrelation functions (ACFs) of the complex time series. Every 5 s 29 measured ACFs are integrated together and stored on disc. For our analysis we additionally summarized 4 such ACFs resulting in an analysis time resolution of 20 s.

The general form of the ACF can be written as (Jackel, 2000; Moorcroft, 2004; Strelnikova and Rapp, 2010; Strelnikova and Rapp, 2011):

$$\mathrm{ACF}(\tau) = \mathrm{ACF}_{\tau=0} \cdot \exp\{-(\tau/\tau_\mathrm{e})^n\} \cdot \exp\{i\ 2\pi\ \delta f\ \tau\}, \quad (1)$$

where ACF is the magnitude of the autocorrelation function, τ is the time lag at which the ACF is evaluated, δf is the phase of the complex autocorrelation function (from which the vertical velocity of the scatterers is derived), τ_e is the correlation time of the ACF (inversely proportional to the spectral width), and the parameter n describes the shape of the spectrum: Lorentzian and Gaussian shapes correspond to $n = 1$ and $n = 2$, respectively, whereas $n < 1$ reflects the presence of charged aerosol (e.g. dust) particles (Rapp et al., 2007).

In the case of a Lorentzian line shape ($n = 1$) the half-power half-width of the spectrum is

$$W_\mathrm{L} = \frac{1}{2\pi\ \tau_\mathrm{e}}. \quad (2)$$

In the case of purely incoherent spectra this value is determined by the lifetime of heavily damped ion-acoustic waves which are excited by thermal fluctuations in the plasma and is given by

$$W_\mathrm{L} = \frac{16\pi k_\mathrm{B}}{\lambda_\mathrm{R}^2} \frac{T}{m_\mathrm{i} \nu_\mathrm{in}}, \quad (3)$$

where k_B is Boltzmann's constant, λ_R is the wavelength of the radar (e.g. 1.34 m), T is the temperature (which we assume to be identical for ions, electrons, particles, and neutrals), m_i is the positive ion mass (which is 31 amu in this manuscript), and ν_in is the ion–neutral momentum transfer collision frequency (e.g. Dougherty and Farley, 1963; Mathews, 1984).

In case of a Gaussian line shape ($n = 2$), τ_e determines the half-power half-width of the Gaussian that reads

$$W_\mathrm{G} = \frac{1}{\pi\ \tau_\mathrm{e}} \cdot \sqrt{\ln(2)}. \quad (4)$$

In general, the following quantities may be derived from the measured ACF: the line of sight (here: vertical) wind velocity, the spectral width (under assumption of Lorentzian), and the spectral shape parameter n.

Furthermore, electron densities are obtained from values of the total backscattered power by means of the "GUISDAP" software package. The such derived apparent electron number densities are converted to volume reflectivities using the well-known relation

$$\eta = \sigma \cdot N_\mathrm{e}, \quad (5)$$

where $\sigma = 5 \times 10^{-29}\,\mathrm{m^2}$ is half the scattering cross section σ_e of an electron ($\sigma = \sigma_\mathrm{e} \cdot (1 + T_\mathrm{e}/T_\mathrm{i})^{-1} = \sigma_\mathrm{e}/2$ for equal electron and ion temperatures, T_e and T_i), and N_e is the (apparent) electron number density (e.g. Röttger and La Hoz, 1990).

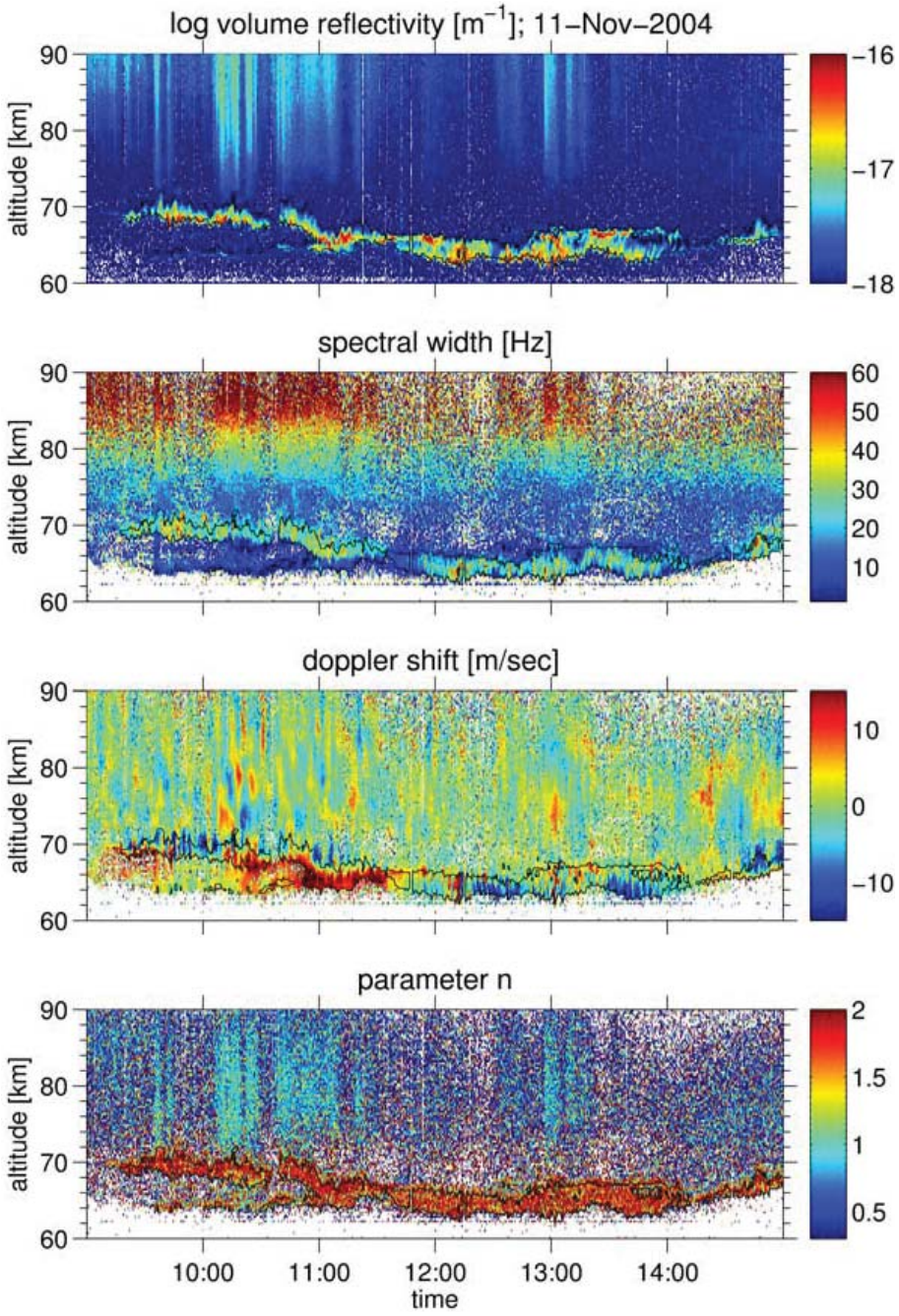

Fig. 1. Example of PMWE observations measured by VHF radar. Panels from top down: volume reflectivity; half-power full-width obtained by fitting Lorentzian ($n = 1$ in Eq. 1) to measured ACF; vertical wind velocity; parameter n (see Eq. 1). Black contours show PMWE layer (i.e. region of increased SNR).

Sample results obtained from VHF radar measurements during a PMWE event, showing all the parameters that can be derived from such observations, are shown in Figs. 1 and 6. These data will be discussed in more detail in the next section.

4 Examples of PMWE measurements with the EISCAT VHF radar

Before we start with a statistical analysis of all PMWE-related available EISCAT data, we would like to discuss two particular events from this database.

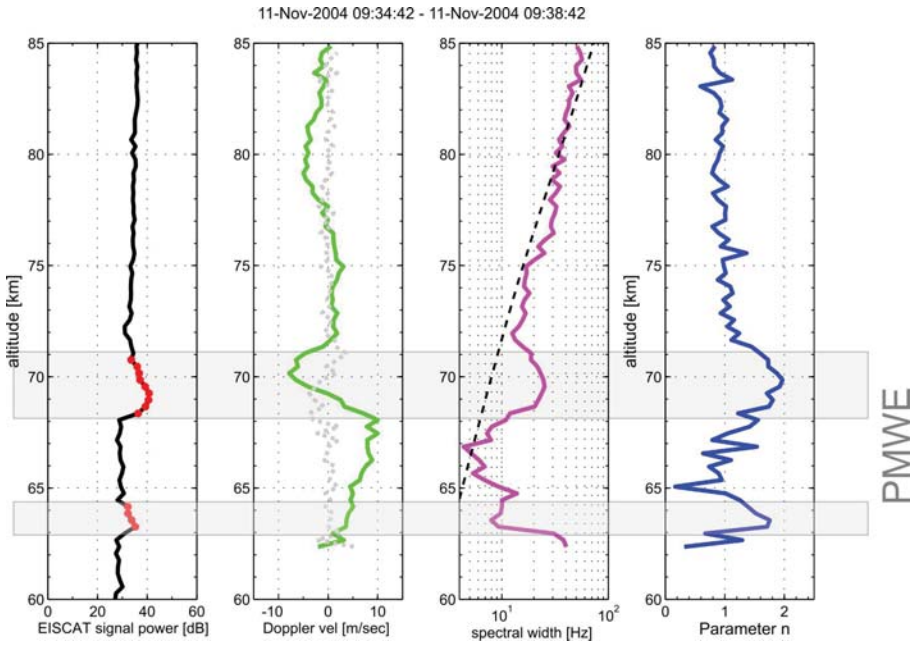

Fig. 2. Altitude profiles for time interval between 09:34 and 09:38 UT. Panels from left–right: SNR (red dots indicate increased values considered as PMWE signal); vertical wind velocity – grey dotted line shows wind difference between two range gates; half-power full-width – black dashed line shows spectral width obtained from Eq. (3) (temperature and neutral density were taken from MSIS-90 Atmosphere Model (Hedin, 1991)); parameter n. Grey boxes show PMWE layers.

The first data set was obtained on 11 November 2004, when a strong PMWE event was observed over a total period of ~ 6 h. An overview of these measurements is shown in Fig. 1. A strong volume reflectivity increase was observed below $\sim$70 km. Inhomogeneous wave-like structures are seen inside the region of increased volume reflectivity (Fig. 1, upper panel). The spectral width (Fig. 1, second panel from top) also reveals inhomogeneous structures, but they are not so wave-dominated as in the case of volume reflectivity. Since the antenna was directed vertically in this case (see Table 1 for more details on the experiment), and the antenna beam is rather narrow, the Doppler shift represents a measure of the vertical movement of the structures in the electron gas which is responsible for the scattering. These Doppler measurements reveal a large activity of short-period waves (with observed periods of 5–10 min) above the PMWE layer. In contrast, observed wave periods inside the PMWE layer are much longer, i.e. mostly larger than 1 h. Furthermore, it is interesting to notice that during most of the time the upper part of the layer is characterized by a change of the vertical wind direction. Finally, the parameter n shows a Gaussian line shape inside the layer and a Lorentzian shape outside. Note that this feature is persistently observed as long as the SNR is large enough to get reasonable results from fitting. We further note that these results are similar to observations of PMSE layers as reported by Strelnikova and Rapp (2010); Strelnikova and Rapp (2011).

Figure 2 shows vertical profiles of the discussed parameters for a time interval of 4 min. In the upper PMWE layer, a large wind gradient can be easily recognized. Above the upper layer the wind fluctuations are weaker. In the same example, we further notice that the spectral width inside the upper layer is factor of ~ 3 larger compared to incoherent spectral widths estimated from Eq. (3). We note that a reliable estimation of the broadening in the lower layer is difficult because an additional broadening takes place due to presence of negative ions in this altitude range (e.g. Mathews, 1978; Rietveld and Collis, 1993; Raizada et al., 2008).

The derived parameters n are close to a value of $n = 1$ outside both layers and approaches $n = 2$ inside the PMWE layers. During this particular day, the median values of the parameter n inside and outside the whole PMWE event are equal to 1.745 and 0.96, respectively (see Table 1 for more details). The same behaviour of the parameter n was found for PMSE events by Strelnikova and Rapp (2010); Strelnikova and Rapp (2011). To our current understanding of PMSE (e.g. Rapp and Lübken, 2004), these echoes are caused by coherent structures in the refractive index that produce the back scattering of a transmitted radio signal. These structures, in turn, are created by neutral air turbulence in combination with an efficient reduction of electron diffusivity by charged mesospheric ice particles (see e.g. Batchelor, 1959; Hill, 1978; Kelley et al., 1987; Rapp and Lübken, 2003; La Hoz et al., 2006; Varney et al., 2011).

Table 1. Results of EISCAT observations over ∼ 32.5 h PMWE observations.

NN	date	PMWE time (in min)	alt (min, max)		el. [deg]	Δ alt [km]	n (in out)		Dop vel $[m\,s^{-1}]$ (in out)		Δ (Dop Vel) $[m\,s^{-1}]$ (in out)		W_L/W_{TH} (in out)		W_G $[m\,s^{-1}]$	ϵ $[mW\,kg^{-1}]$
1	1 Nov 2003	08:31 08:59 (21 min = 0.35 h)	66.26	68.66	90	0.300	1.2752	0.9595	1.90	0.0031	0.0253	4.528e − 03	0.8350	0.7231	2.409	29.37
2	1 Nov 2004	09:44 11:29 (88.5 min = 1.5 h)	61.46	63.86	90	0.300	1.6592	1.3749	0.32	0.4058	0.0147	−4.679e − 02	1.4193	1.0348	1.989	19.61
3	2 Feb 2008	09:41 12:13 (24.3 min = 0.4 h)	60.26	71.66	90	0.300	1.6139	0.9847	0.90	−0.2897	0.0445	−6.389e − 02	0.6802	0.5786	2.177	25.23
4	2 Nov 2003	05:03 07:45 (61.67 min = 1.03 h)	66.26	75.26	90	0.300	1.3731	0.9740	0.33	0.1487	−0.0662	5.263e − 03	1.3617	0.6415	6.877	265.77
5	3 Feb 2008	10:33 12:15 (14.2 min = 0.24 h)	65.06	75.56	90	0.300	1.7034	0.9591	0.13	−0.0812	−0.0676	−1.237e − 02	0.5541	0.5413	2.919	48.31
6	4 Feb 2008	09:39 11:27 (12.8 min = 0.21 h)	60.26	70.76	90	0.300	1.7551	0.9479	−0.03	0.4530	−0.4558	7.793e − 02	0.9191	0.6120	2.604	35.24
7	5 Feb 2008	09:29 11:28 (28.6 min = 0.5 h)	60.26	70.46	90	0.300	1.7493	1.5221	0.39	2.5432	−0.1153	*NaN*	1.9513	0.9126	5.310	148.24
8	9 Nov 2004	11:18 12:32 (24 min = 0.4 h)	62.36	63.86	90	0.300	1.6188	0.9446	1.80	−0.0109	−0.0879	−9.262e − 03	1.6506	1.0530	2.393	28.57
9	10 Nov 2004	08:05 12:11 (97 min = 1.6 h)	62.70	67.50	90	0.300	1.5184	0.9839	0.95	0.0038	0.0608	−4.238e − 03	2.1359	1.1570	3.836	73.27
10	10 Nov 2004	19:11 23:35 (89 min = 1.5 h)	67.50	73.80	90	0.300	1.3373	0.9823	−2.17	0.0099	0.0974	1.182e − 02	3.5487	1.1710	12.942	879.08
11	11 Nov 2004	08:04 15:02 (391.3 min = 6.5 h)	60.26	70.76	90	0.300	1.7500	0.9810	1.15	0.0658	−0.0967	8.505e − 03	4.0650	1.0547	8.038	325.09
12	12 Nov 2004	07:01 16:37 (302.3 min = 5.04 h)	61.46	75.56	90	0.300	1.7020	1.0044	2.40	0.1754	−0.0523	−1.412e − 04	2.0330	0.8082	6.003	185.96
13	13 Nov 2004	12:06 13:40 (21.3 min = 0.356 h)	60.00	64.20	90	0.300	1.8112	1.0113	−3.51	1.6101	0.3977	7.322e − 03	3.1730	0.6960	4.474	99.97
14	17 Jan 2005	12:12 13:18 (34 min = 0.57 h)	58.75	68.80	80	0.295	1.3455	0.9482	8.39	2.7901	−0.1451	−6.828e − 02	1.2784	0.8203	3.979	80.37
15	21 Jan 2005	09:52 13:27 (25 min = 0.42 h)	60.26	73.46	90	0.300	1.2211	1.0905	−0.72	0.0007	0.0168	−4.742e − 03	1.0572	0.8013	3.575	65.81
16	21 Nov 2003	11:15 12:51 (70.67 min = 1.18 h)	65.96	70.76	90	0.300	1.7820	0.9693	0.64	−0.4098	0.0746	−2.331e − 02	3.3257	0.7948	8.107	336.96
17	24 Nov 2006	08:31 09:55 (18 min = 0.3 h)	62.66	71.36	90	0.300	1.6072	0.9550	0.80	0.3439	−0.1254	2.907e−02	1.5740	0.7454	4.093	86.86
18	24 Oct 2006	10:38 11:49 (58.67 min = 0.98 h)	60.26	71.66	90	0.300	1.6115	1.2996	0.83	0.2060	−0.0256	−6.975e − 01	0.9073	0.5553	2.478	31.25
19	27 Nov 2006	10:01 11:26 (8.53 min = 0.14 h)	68.06	71.06	90	0.300	1.7616	0.9596	−3.16	0.2649	0.1218	1.797e − 02	1.5249	0.7101	5.239	143.63
20	28 Nov 2006	11:12 11:45 (15.67 min = 0.26 h)	60.26	72.56	90	0.300	1.5742	1.0971	1.60	1.0084	−0.6625	−1.708e − 02	1.0141	0.6797	4.123	89.81
21	28 Oct 2003	09:10 14:20 (81 min = 1.35 h)	60.26	68.96	84.3	0.300	1.6568	0.9877	1.21	−0.0902	0.1316	−6.823e − 03	2.3005	0.7435	4.131	84.71
22	29 Oct 2003	08:42 09:17 (23.7 min = 0.4 h)	59.16	64.80	70	0.282	1.2185	1.0512	−0.63	2.1225	0.0366	9.436e − 02	3.8339	1.1636	5.326	140.53
23	29 Oct 2003	12:47 14:59 (39.3 min = 0.66 h)	56.14	68.36	60	0.260	1.6142	1.0735	4.47	2.6278	0.0409	1.881e − 01	4.4859	1.3823	7.338	274.05
24	29 Oct 2004	12:45 14:00 (25.7 min = 0.43 h)	63.26	67.76	90	0.300	1.5274	1.4578	−0.01	0.0146	−0.3580	1.021e − 01	1.0238	0.7798	2.924	43.54
25	30 Oct 2003	06:29 14:45 (344.7 min = 5.7 h)	65.62	78.81	72.9	0.287	1.5425	1.0866	−2.30	−9.5772	−0.4044	3.290e − 02	1.2990	0.4657	5.099	139.46
26	31 Oct 2003	13:18 13:56 (18.3 min = 0.3 h)	65.08	68.18	70	0.282	1.3615	1.2162	−8.65	0.0005	0.1628	−4.859e − 02	0.9530	0.6858	2.463	30.87

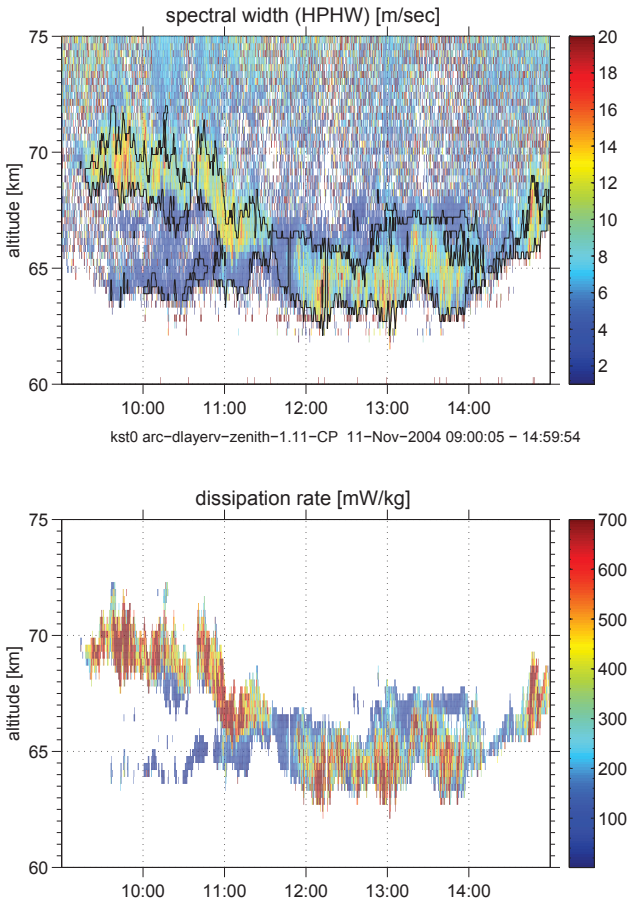

Fig. 3. Upper panel: spectral width derived under assumption of Gaussian-shaped spectra (i.e. $n = 2$ in Eq. 1). Lower panel: energy dissipation rates inside the PMWE layer.

Thus, it is possible to visualize the turbulent structures in the IS measurements of PMSE by introducing the parameter n in the analysis. Since we observed a similar behaviour in PMWE measurements, we can make a similar analysis of the measured data as it was done for PMSE. That is, assuming that scattering inside the layer is related to neutral air turbulence, we can fit a Gaussian to the measured data and derive spectral width using Eq. (4). From this value the energy dissipation rate ϵ can be estimated following Hocking (1985) and Röttger et al. (1990):

$$\epsilon = \frac{0.4 W_G^2 N}{2 \ln 2}, \tag{6}$$

where W_G is the half-power half-width of the Gaussian Doppler spectrum (in $\mathrm{m\,s^{-1}}$), and N is the buoyancy frequency which we derive from the MSISE90 model (Hedin, 1991).

Corresponding results are shown in Fig. 3. The upper panel shows the half-power half-width obtained from Eq. (4). The lower panel shows the resulting energy dissipation rates. The obtained values are considerably larger than those reported by Lübken et al. (1993b). Large ε values during PMWE events have been repeatedly observed (e.g. Collis et al., 1992; Lübken et al., 2007; Kirkwood et al., 2006b; Brattli et al., 2006). Note also that Lübken et al. (2006) reported smaller spectral widths (their Fig. 12) measured with the ALWIN VHF radar. Note that this radar has a broad beam in comparison to the EISCAT VHF radar where beam broadening effects are essentially negligible (Strelnikova and Rapp, 2011). This analysis implies very strong turbulence during this special event. Notably, enhanced turbulence activity during this time period, i.e. 8 to 13 November 2004, was also reported by Hall et al. (2007) based on MF radar observations. It is further interesting to note that the Davis MST Radar in Antarctica (68.6° S, 78.0° E) also measured peak PMWE intensity on 11 November 2004 (Morris et al., 2011). That is, a very strong PMWE event was observed simultaneously in both hemispheres.

The patchy spectral width inside the PMWE layer is reminiscent of similar typical structures which are often seen in PMSE. In contrast, the IS spectral width increases smoothly exponentially with altitude. However, as opposed to PMSE, the spectral width is increased inside the PMWE layer (e.g. Collis et al., 1992; Lübken et al., 2006).

Since the EISCAT beam was pointed vertically, it is not possible to infer any information about horizontal winds from these measurements. However, wind measurements are available from the Saura MF radar located in Andenes (∼130 km apart). Figure 4 shows vertical, zonal, and meridional winds measured on 11 November 2004 with the Saura MF radar. Black contours mark the location of the PMWE layer as observed by the EISCAT radar. From these data we estimated the total (squared) wind shear as $(\mathrm{d}u/\mathrm{d}z)^2 + (\mathrm{d}v/\mathrm{d}z)^2$, where u and v are the zonal and meridional wind components, respectively, and z is the vertical coordinate. The results are shown in Fig. 5. The wind shear is a measure of the energy available to drive turbulence. The Richardson number, Ri, which is the ratio of buoyancy frequency squared (N^2) to the wind shear is the parameter commonly used to assess the chance that turbulence can be initiated (if $Ri < 0.25$) or that it can be maintained (if $Ri < 1$). The buoyancy frequency N varies between 1.7×10^{-2} and $2.3 \times 10^{-2}\,\mathrm{s^{-1}}$ in the mesosphere (Belova et al., 2005; Kirkwood, 2007; Rapp et al., 2011). That is, $N^2 \sim 10^{-4}$ is two orders of magnitude smaller than the wind shear, which ranges between 2 and $15 \times 10^{-2}\,\mathrm{s^{-2}}$. Thus, below ∼ 70 km between 08:00 h and midday the atmosphere was dynamically unstable, i.e. $Ri << 0.25$. During this time EISCAT observed the strong PMWE layer, which is indicated by the pink contour.

The next example that we would like to discuss in this paper was observed one day before, i.e. on 10 November 2004. This event has already been analyzed by Kirkwood et al. (2006b) and Lübken et al. (2007). An overview of these measurements is shown in Fig. 6. The PMWE event observed during this day is characterized by a rather weak signal which lasted for a much shorter time period than during

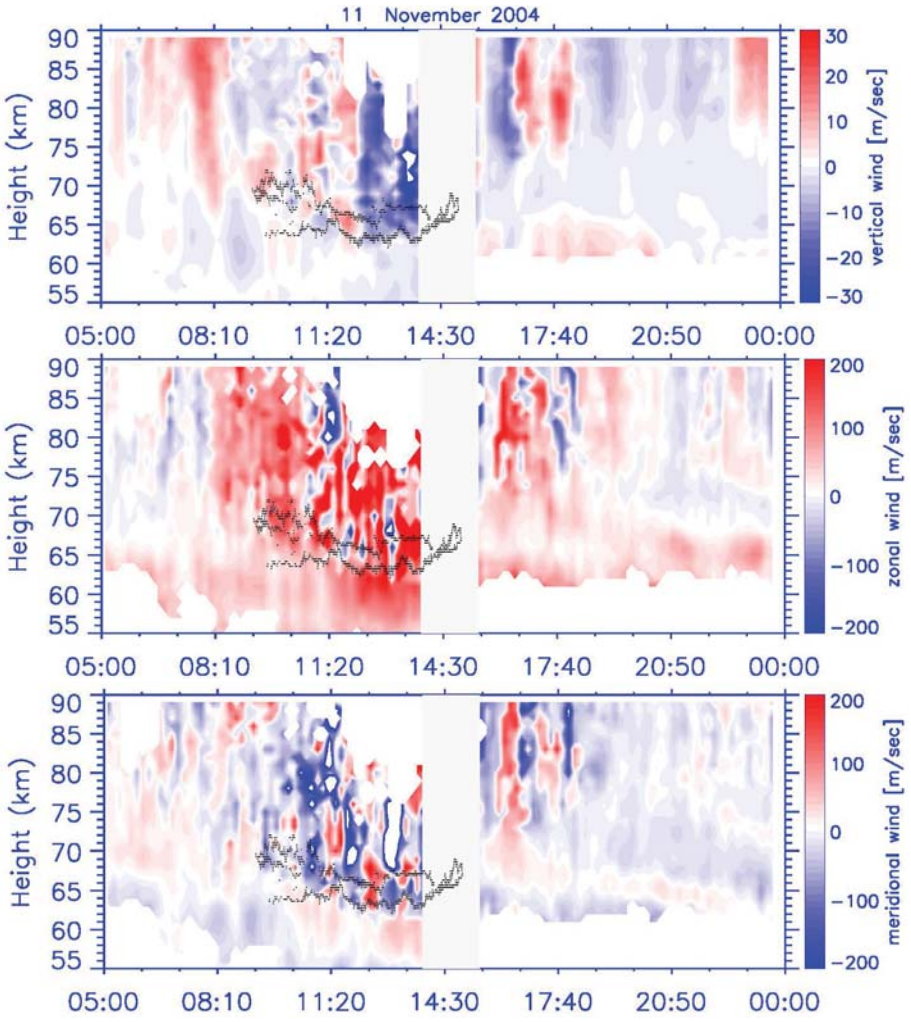

Fig. 4. Saura MF radar wind measurements. Panels from top down: vertical (upwards), zonal (from the west), meridional (from so the north) winds. Black contours show simultaneous EISCAT PMWE measurements. In brackets positive wind direction is shown.

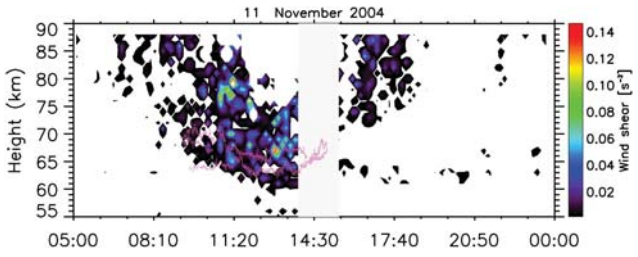

Fig. 5. Saura MF radar wind shear measurements. Pink contour marks PMWE layer observed by the EISCAT radar.

the following day. Similar to the previous example, wave-like structures are clearly seen in the volume reflectivity. Also, a spectral width increase inside the PMWE layer can only be noted until 08:30 UT, after which spectral widths inside and outside the layer appear to be identical. This fact led Kirkwood et al. (2006b) (who showed EISCAT spectra averaged from 08:36 to 08:42 UT) to the conclusion that turbulence can be excluded as a possible source of PMWE.

We analyze the same data but choose a slightly different integration time and show the altitude profile of our fitting results in Fig. 7. Each of the three panels shows a 3-min average. The upper plot shows results obtained from 08:37 to 08:40 UT. Indeed, the spectral broadening in this time interval is difficult to recognize. This is similar to the lower layer, shown in Fig. 2, where broadening due to negative ions smears out any visible broadening effect from PMWE. Vertical wind inside the layer reduces from 10 to 0 m s^{-1}.

Next, we analyze two additional events, namely measurements from 08:50 to 08:53 UT and between 08:56 and 08:59 UT, i.e. 10 min later than the first example. The results are shown in the middle and lower panels of Fig. 7. Both plots clearly show a weak but distinct broadening around PMWE layer. Note that this weak broadening is not visible in the colour plot in Fig. 7. From these plots we may further

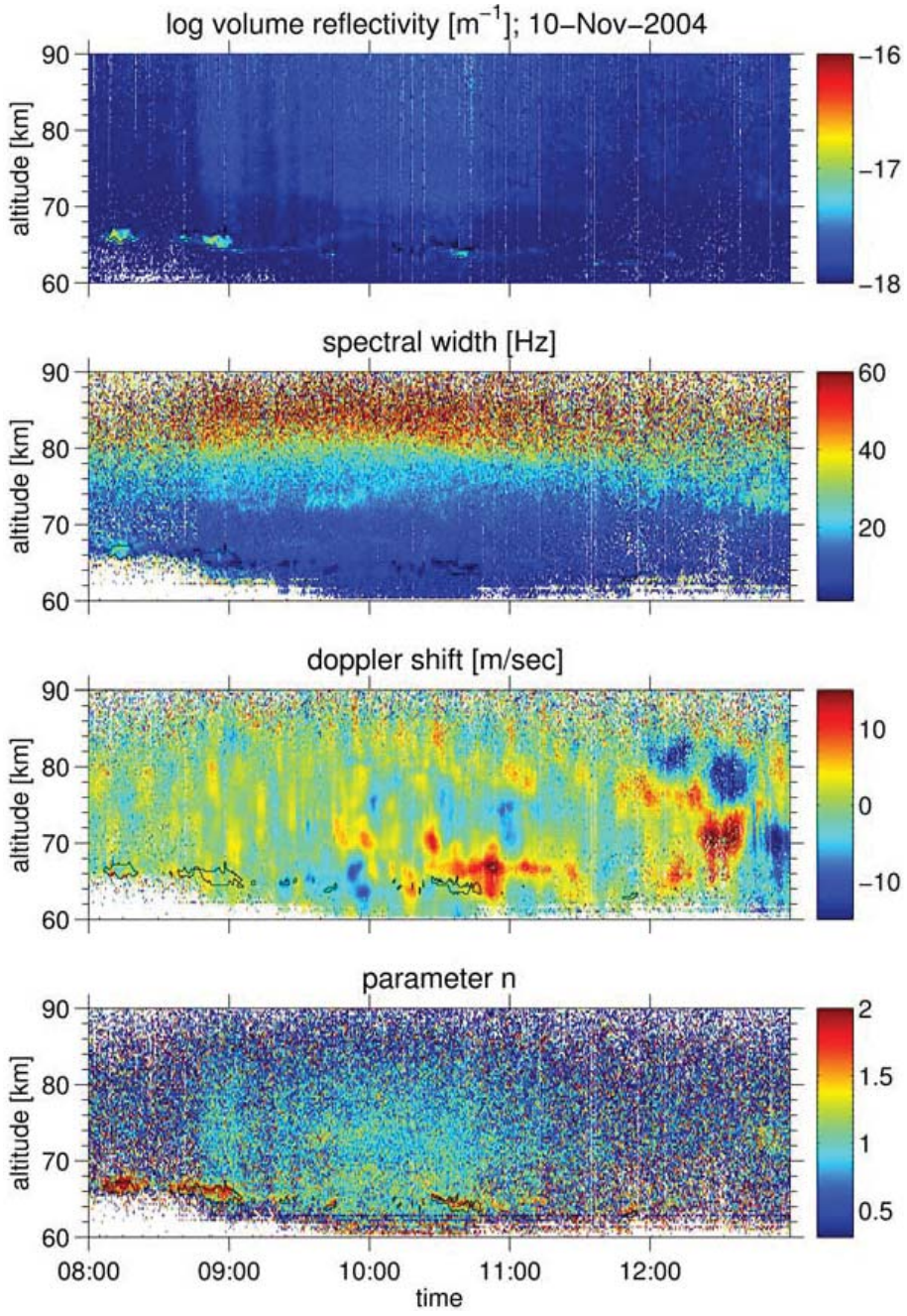

Fig. 6. The same as Fig. 1, but for 10 November.

estimate that spectral broadening due to negative ions occurs up to altitudes of about 65 km. Thus, broadening above $\sim$ 65 km during 08:37 to 08:40 UT could be also due to weak turbulence. However, it is unfortunately not possible to unambiguously determine the origin of the spectral width if it is not considerably larger than the incoherent background. In order to identify the nature of the scatter we thus use the parameter n. The lower panel of Fig. 7 clearly shows coherent structures inside the layer and an incoherent background outside. Thus, we may again interpret the spectral width measurements in terms of turbulent energy dissipation rates and we infer a median ε value of 73 mW kg^{-1}. This value is indeed much smaller than observed during the previous day (see Table 1).

The vertical wind inside the PMWE layer is weak and does not reveal strong gradients as in the previous example. Similar to Fig. 1, some small-scale wave activity is seen above the layer. Also, wind measurements with the SAURA MF radar

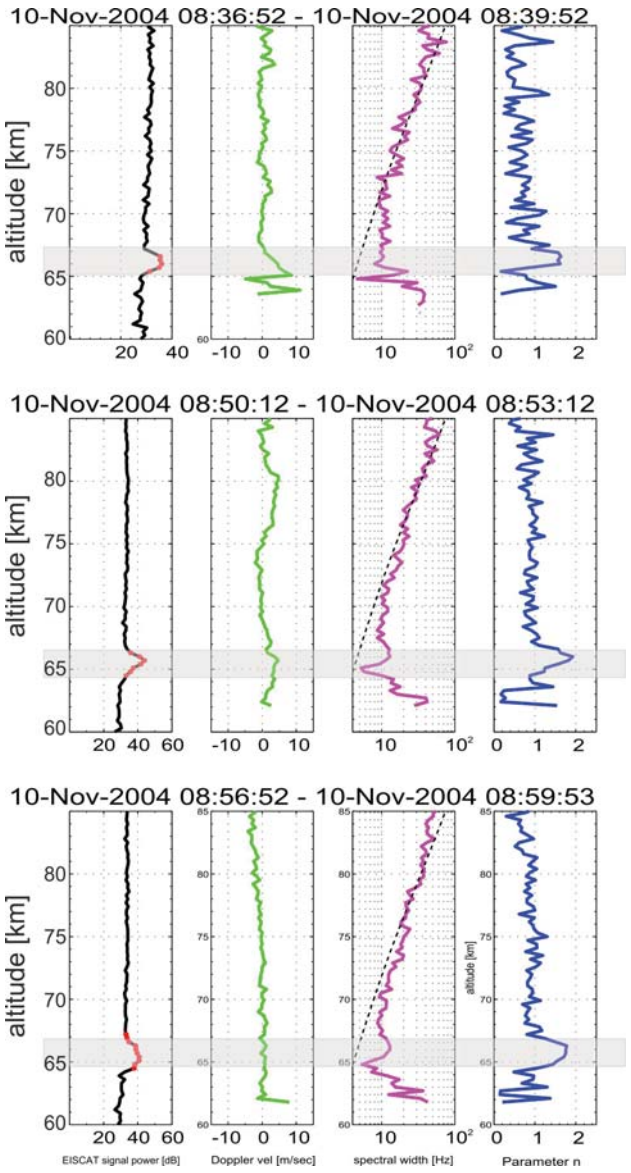

Fig. 7. Similar to Fig. 2, but for 10 November 2004 and for 3 different time intervals. Exact times; see in plot headers and in the text.

reveal smaller wind values (see Fig. 8) compared to the next day (i.e. 11 November). In addition, the wind shear is of the same order of magnitude as the buoyancy frequency squared (N^2). Thus, this second example demonstrates a weak event without strong turbulence and pronounced features.

These two extremely different PMWE events occurring within the very short period of only two days motivated us to analyze a much larger data set in order to retrieve typical PMWE features that are statistically significant.

5 Statistical results

We analyzed a total of ~ 32.5 h of PMWE observations with the EISCAT VHF radar. Details of these observations and a short overview are listed in Table 1. In the first column the date of observations is indicated. The next column states the time of the PMWE display (i.e. when PMWE was observed and also the duration of the event). Note that these times represent the beginning and the end of the event, even if the PMWE display was discontinuous during that time. However, the duration of events was calculated without gaps in the PMWE display; that is, it reflects only the times when PMWE was observed.

The next column shows the altitude of the PMWE. This reveals that all PMWE events were located between 56 and 79.67 km.

Since measurements in October 2003 were conducted with a tilted beam, we also show the beam elevation and altitude resolution in the next two columns of Table 1.

The last 6 columns represent the following analysis results:

– Median value of the parameter n inside and outside the PMWE layers: in all examples $n > 1$ inside the layers and $n \simeq 1$ outside. Only two days reveal comparable values inside and outside the PMWE layers (NN 24, 26). On 29 October 2004 (NN 24) SNR was very low. Small sporadic power increases around the PMWE produce artefacts in the analysis outside the layer which can be mixed up with PMWE. However, this was statistically unimportant compared to the large number of other examples. The layer detected on 31 October 2003 was very weak, so that the boundary of this layer could not be clearly defined.

– Median doppler velocity in $\mathrm{m\,s^{-1}}$ inside and outside the layers: in most cases the absolute value of the median doppler velocity is larger inside the layer than outside. This is not the case for 4 February 2008, where wind measurements were available well above the higher layer (~ 10 km apart). This finding also does not apply for a tilted beam. Also, in some cases SNR outside the layers was too low and, therefore, the statistics for median values are not appropriate. A better representation by histograms will be given further below in this manuscript.

– Doppler velocity difference between two altitudes in $\mathrm{m\,s^{-1}}$ inside and outside the layers (in order to get velocity gradient this value has to be divided by the corresponding altitude resolution): in most cases this (absolute) value is larger inside the layers than outside.

– Ratio of spectral width, obtained by fitting a Lorentzian ($n = 1$ in Eq. 1) to the measured ACF, to theoretical one estimated from Eq. (3), where temperature and neutral

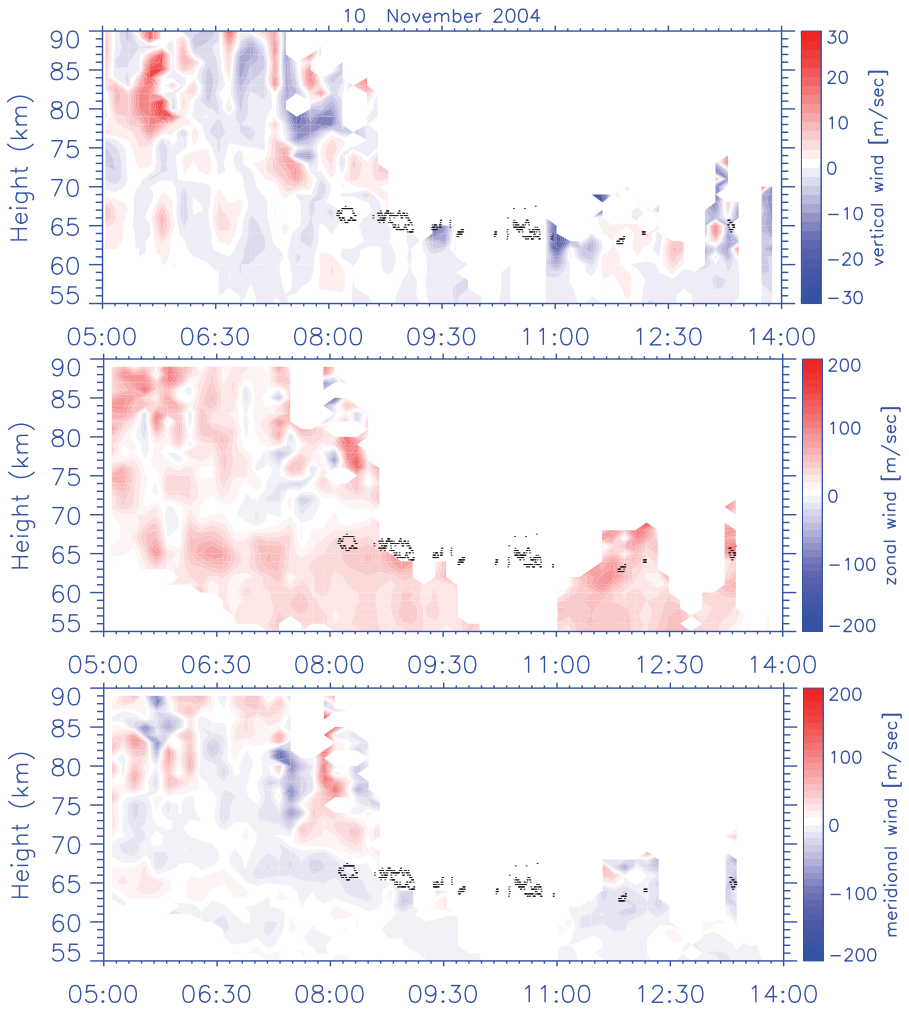

Fig. 8. The same as Fig. 4, but for 10 November 2004.

density were taken from MSIS-90 model: these median values inside and outside the layers represent broadening inside the layer in comparison to background conditions. In most cases this ratio reveals larger values inside the layer. In some cases, like NN 11, 13, 23, this difference is extremely large.

– Half-power half-width of the Gaussian in $m\,s^{-1}$ inside the layer (median): comparison of this value inside and outside the layer makes no sense because outside the layer spectral shape reveals Lorentz shape; spectral width exponentially increases with altitude and in lower altitudes the signal comes generally from PMWE, thus spectral width obtained outside the layer is usually larger than inside. Comparison of spectral width outside the layer, but at the same altitudes as PMWE signal, reveal very poor statistics.

– Energy dissipation rates inside the PMWE layer estimated from Eq. (6) (median): Note that the dissipation rate was estimated for every particular measurement, where dependence of buoyancy frequency on altitude was taken into account. Our results do not exactly agree with a finding of Kirkwood et al. (2006b), where they found for 10 November 2004 a spectral width of $\sim$7 Hz = 4.7 $m\,s^{-1}$ for the morning event (NN 9 in Table 1) and $\sim$ 20 Hz = 13.4 $m\,s^{-1}$ for evening event (NN 10). From these values they estimated energy dissipation rate in the ranges 75–100 $mW\,kg^{-1}$ and 600–800 $mW\,kg^{-1}$, respectively. For HPHW we obtained a median value of 3.8 $m\,s^{-1}$ for the layer in the morning, which is $\sim 1\,m\,s^{-1}$ smaller than the value reported by Kirkwood et al. (2006b). But our estimate of the dissipation rate of 73.3 $mW\,kg^{-1}$ stays close to the range estimated by these authors. For the evening event we derive a spectral width of 13 $m\,s^{-1}$, which is in agreement with Kirkwood et al. (2006b), and a dissipation rate of 880 $mW\,kg^{-1}$, which exceeds the upper limit estimated by Kirkwood et al. (2006b).

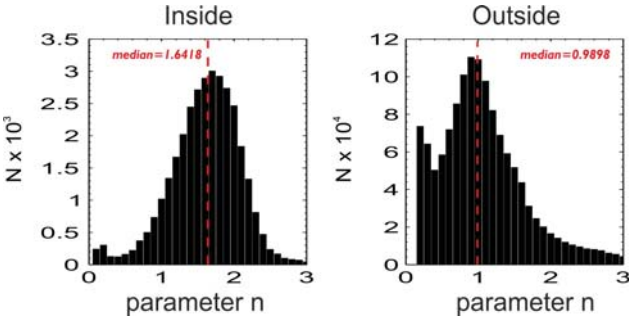

Fig. 9. The statistics done from 32.5 h EISCAT PMWE observations. Left panel shows the distribution of spectral shape (determinated by parameter n) inside of PMWE layers. Right panel – outside of PMWE layers.

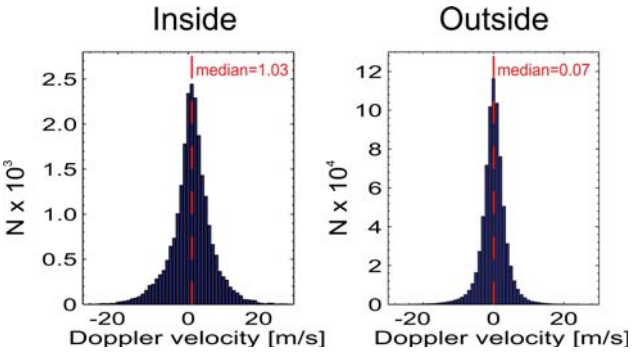

Fig. 10. The statistics of vertical wind observations. Left panel shows the distribution inside of PMWE layers. Right panel – outside of PMWE layers.

Since we have shown in Figs. 1, 3, and 6, that all the parameters shown in Table 1 are highly variable; it is useful to represent their distributions in the form of histograms.

Figure 9 shows distribution of the spectral parameter n inside and outside the PMWE layers. As expected the median value outside the layers $\simeq 1$. This means that these D-region IS spectra are Lorentzian (as expected) in the absence of PMWE. This histogram further shows that some spectra reveal extreme spectral parameters, i.e. $n \ll 0.5$ or $n \geq 2.0$. These values come from the regions of lower SNR or from the upper boundary of observations (see lowermost panel in Figs. 1 and 6 above ~ 85 km). Inside the PMWE layers the parameter $n > 1.0$ in 91.4 % of all measurements and the median value is ~ 1.64. Interestingly, this value is close to the value derived from UHF Radar measurements of PMSE events (Strelnikova and Rapp, 2011). This is probably because the signal increase during VHF PMWE events is of the same order of magnitude as in the case of UHF PMSE (i.e. weak compared to VHF PMSE).

The weak radar signal, that is, the low SNR, leads to the following difficulties in the data analysis:

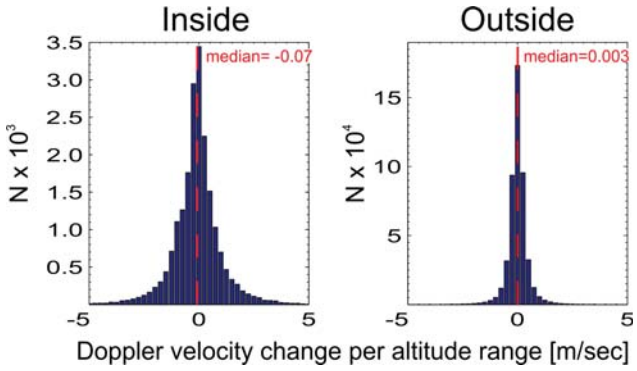

Fig. 11. The statistics of gradient in vertical wind observations. Left panel shows the distribution inside of PMWE layers. Right panel – outside of PMWE layers.

– It is difficult to unambiguously define a spectral shape (fitting error is large because of the scatter of the measured ACF points).

– It is possible that the backscattered signal results from a superposition of coherent and incoherent scattering.

Figure 10 shows distribution of vertical wind measurements inside and outside the PMWE layers. Note that for this and further statistics we have only used measurements with the vertical beam because doppler wind measurements with the tilted beam are caused by a superposition of vertical and horizontal winds. Also, the spectra are broadened when the antenna is directed off-vertical (e.g. Collis and Rietveld, 1998).

The vertical wind measurements reveal a median value of 1.03 inside the layers and 0.07 m s^{-1} outside. Also, the wind distribution inside the layers is broader (Fig. 10). The standard deviation is 6 and 4 m s^{-1} inside and outside the layers, respectively. For comparison, Kirkwood et al. (2006b) also showed (based on analysis of only two PMWE layers) that the mean Doppler shift is zero outside PMWE and varies between -2 to -3 and $+4$ to $+5$ s inside.

Distributions of the vertical wind gradient shown in Fig. 11 reveal quite similar behaviour to those of the vertical wind. Namely, inside the layers they show a broader distribution and a nonzero median value (i.e. 0.07 [m s^{-1}]/300 [m] inside and 0.003 [m s^{-1}]/300 [m] outside the layer). Outside the layers 6 % of all the measurements reveal a vertical wind change which is larger than 1 m s^{-1} over one altitude bin. Inside the layer this value increases to 20 %. Under normal conditions gravity waves produce wind fluctuations. The amplitude of these fluctuations can be seen in right panel of Fig. 11, i.e. outside the PMWE layers. Inside the layers wind fluctuations and gradients are larger.

A comparison of spectral widths is shown in Fig. 12. Since spectral width is a function of altitude, we use a ratio of the measured spectral width (Eq. 2) to the theoretical spectral width (Eq. 3). Inside the PMWE layers this value reveals a much broader distribution (left panel) than outside (middle

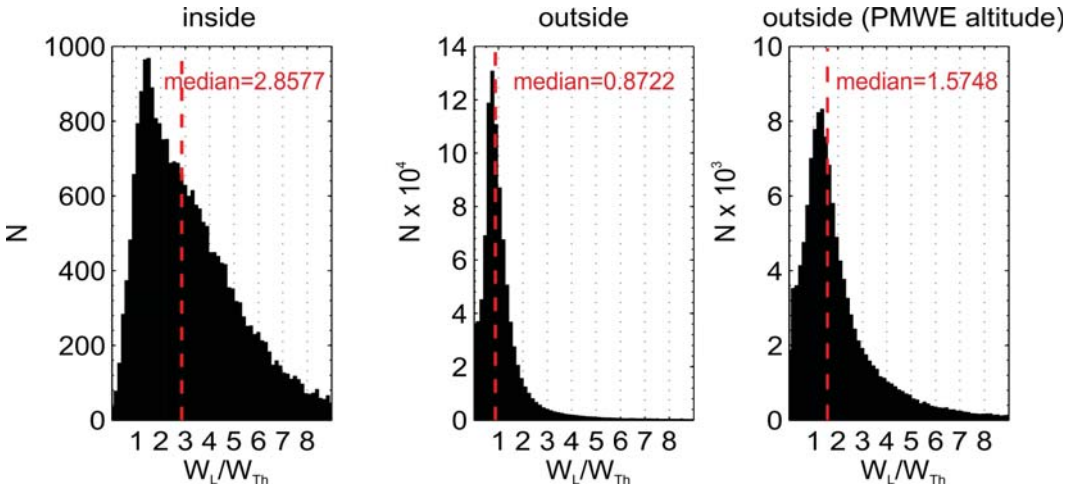

Fig. 12. Statistics of ratio of measured to theoretical spectral width. Left panel shows the distribution inside of PMWE layers. Middle panel – outside of PMWE. Right panel – outside of PMWE layers, but in altitude range where PMWE occur.

panel). We also have to keep in mind that PMWE occur at rather low altitudes, where spectral broadening due to negative ions occurs and we do not take into account this broadening in our theoretical estimation of spectral width. In order to analyze this broadening effect further, we picked out values from the non-PMWE distribution which lie in the same altitude range as the PMWE layers. Results are shown in the rightmost panel of Fig. 12. Notably, also this distribution is not as broad as inside the layers. Note that the spectral width inside and outside the PMWE layers is not an artefact. Of course, measurements of spectral width with low SNR will result in a broader distribution, but this is not the case in our study. SNR inside the layers is higher than the background SNR (at least at the same altitudes: right and left panels of Fig. 12), so the estimation of spectral width must be more accurate inside the layers than outside the layers. The middle panel serves as a measure of data quality on the one side (i.e. how strong the fluctuations are), and comparability of theoretical estimations with experiment on the other side. It is well known that spectral width derived from IS radar data reveals smaller values than expected from theory (Hansen et al., 1991; Rietveld and Collis, 1993; Rapp et al., 2007). Our data set results in a median value of ~ 0.87 and is in a good agreement with previous estimates. The measurements from lower altitudes (right panel) reveal a median value of ~ 1.6, which is larger than 1, but still smaller than ~ 2.9, i.e. the median value inside the PMWE layer. Thus, our statistical analysis indicates a larger spectral broadening inside the PMWE layers (i.e. larger median values and broader distribution) than outside the layers – even after taking into account the broadening effect of negative ions.

Kirkwood et al. (2006b) also reported a broader distribution of spectral width inside the PMWE layer (their Fig. 4, item No. 9 in Table 1) with a maximum of the distribution at $\sim 4\,\mathrm{m\,s^{-1}}$ inside the layer and at $\sim 2\,\mathrm{m\,s^{-1}}$ outside. Their Fig. 7 represents the spectral width distribution from the evening PMWE event (item No. 10 in Table 1). This layer lies higher than the previous one (68–74 km). Both distributions (inside and outside) are broad because of the broad IS spectra in this altitude range. The maximum of the distribution is at ~ 8–$11\,\mathrm{m\,s^{-1}}$ inside the layer and at ~ 6–$9\,\mathrm{m\,s^{-1}}$ outside. Note that the IS spectral widths obtained in our analysis using Eg. (3) vary between 2 and $4.5\,\mathrm{m\,s^{-1}}$ for the altitude range between 68 and 74 km. Thus, as explained in Sect. 4, the measured spectral width is broadened due to negative ions, but the median value is consistently larger inside the layer than outside.

6 Discussion

Assuming that the PMWE signal comes from coherent structures created by turbulence, we derive spectral widths from Eg. (4) and estimate energy dissipation rates from Eq. (6). The corresponding results are shown in Fig. 13. The median value of the HPHW is $\sim 6.8\,\mathrm{m\,s^{-1}}$ and the median value of the energy dissipation rate is $\sim 238.5\,\mathrm{mW\,kg^{-1}}$. This value is larger than reported by Lübken et al. (2007) and Kirkwood et al. (2006a) during PMWE events. Also, in situ measurements in the winter mesosphere without PMWE (Lübken et al., 1993b; Lübken, 1997a) reveal considerably smaller ϵ values. Thus, our results reveal extremely high values of turbulent energy dissipation rates, especially for wintertime.

One possible explanation could be that during PMWE events some layers are indeed accompanied by extremely strong turbulence and cause the strong radar return. Previous investigations of PMWE also noted the requirement of very strong turbulence inside the layers in order to explain such strong radar return (Stebel et al., 2004; Brattli et al., 2006).

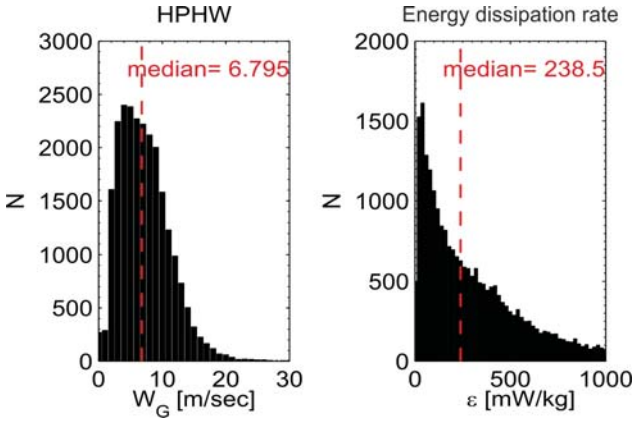

Fig. 13. Left panel shows the statistics of measured Gaussian-shaped spectral width (Eq. 4) inside PMWE layers. Right panel shows energy dissipation rates obtained from measured Gaussian-shaped spectral width (Eq. 6).

Table 2. Heisenberg inner scale [m] estimated for November, 69° N, 19° E.

energy dissipation rate	altitude [km]:		
ϵ [mW kg^{-1}]	60	70	80
ϵ_{min}	21.8	40.3	76.35
10	2.7	6.2	15
100	1.5	3.5	8.6
1000	0.86	1.96	4.84

Another question that we would like to address here is the applicability of Eq. (6) to the measured spectral width. First, we estimate the Heisenberg inner scale of turbulence (Kolmogoroff, 1941; Heisenberg, 1948) for wintertime at 60, 70, and 80 km altitude, following (Lübken et al., 1993a) for different energy dissipation rates: $\epsilon_{\min}$ (lower limit estimation of ϵ, see Eq. 13 from Lübken, 1997b), 10, 100 and 1000 mW kg^{-1}. Results are shown in Table 2. All the derived values exceed the Bragg scale of the EISCAT VHF radar (i.e. 0.67 m). This means that the scatterers have spatial scales which lie in the viscous subrange of the turbulence spectrum. According to Hocking (1985); Hocking and Röttger (1997), the eddies of such scales tend to be very short-lived, intermittent and fragmented, and tend to decouple from the larger eddies. They do not follow the motion of the larger eddies and this process is worst at the smaller scales, and Eq. (6) is probably inappropriate at the scales well within viscous range of turbulence.

In addition, Stebel et al. (2004) estimated radar volume reflectivities from turbulence theory (their Fig. 2) and concluded that turbulence alone cannot account for the strength of the radar echoes measured by the EISCAT VHF radar unless some agent (such as charged aerosol particles, presumably meteoric smoke) reduces the attenuation of turbulent

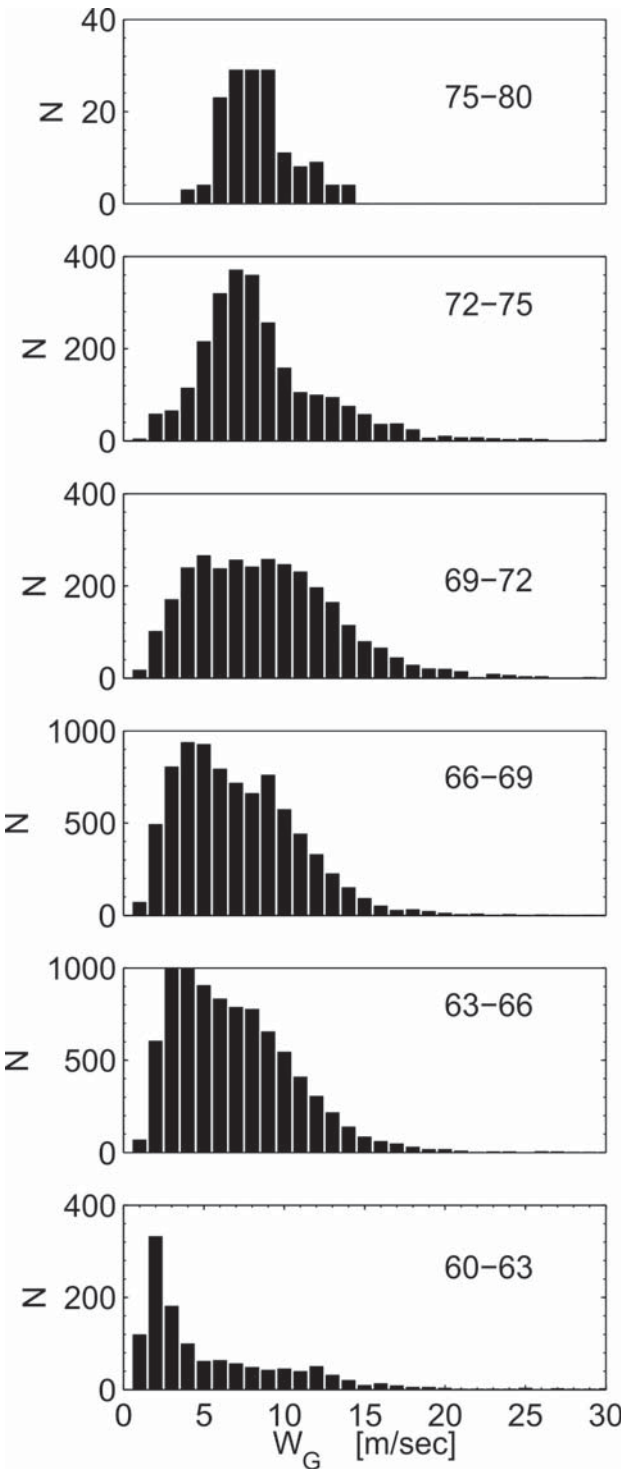

Fig. 14. Gaussian spectral half-power half-widths (HPHW) for different altitude ranges.

fluctuations at small scale sizes. Indeed, an increased amount of larger meteoric smoke particles (i.e. larger than 1 nm) is expected to take place during wintertime in altitude range 50–75 km (Megner et al., 2008). This is in line with findings

of Belova et al. (2008); La Hoz and Havnes (2008), who confirmed the presence of charged dust particles inside PMWE layers by means of artificial RF heating. In addition, Lübken et al. (2006) presented calculations (their Fig. 6) showing that volume reflectivities at the EISCAT VHF radar wavelength can be up to $10^{-13}\,\mathrm{m}^{-1}$ if charged particles with 4 nm radii are assumed. A volume reflectivity of $10^{-13}\,\mathrm{m}^{-1}$ is already larger than any of our observations (see upper panels of Figs. 6 and 1). This implies that the presence of even smaller particles can likely explain the strong measured signals.

In the presence of charged smoke particles of nanometer size, like in PMSE, the electrons are low diffusivity tracers (Kelley et al., 1987; Cho et al., 1992; Rapp and Lübken, 2004; Rapp et al., 2008). For such tracers it has long been known from the studies of Batchelor (1959) that their power spectrum extends to much smaller scales than the spectrum of the turbulent velocity field itself. This happens because the shear at the smallest existing scales in the velocity field leads to a deformation of the tracer distribution which is not (or not sufficiently) counteracted by molecular diffusion. Thus, in such a scenario the inner scale of turbulence in neutral gas is not a crucial value for PMWE measurements and we can use Eq. (6) in a similar approach as for PMSE measurements (Rapp et al., 2008; Li et al., 2010; Strelnikova and Rapp, 2011). Nevertheless, we have to state here that no theoretical validation of Eq. (6) has been done for such conditions with two diffusion modes. Probably some subtle corrections have to be used to convert measured spectral width to energy dissipation rates. Since this question is out of the scope of this work, we only notice this fact as a potential error resulting in an overestimation of energy dissipation rates.

Another potential cause for an of overestimation is a possible mixture of coherent and incoherent signals. Strelnikova and Rapp (2011) considered the possibility that in the case of weak coherent signal embedded into incoherent spectra, some intermediate spectra can be observed. In such cases the parameter n approaches a value of ~ 1.5. For example, if we consider item No. 10 from Table 1, the median value of the parameter n is 1.3 and the energy dissipation rate is highest in the whole observation period. Thus, a possible explanation of the broad spectra could be not very strong turbulence, but a superposition of incoherent and coherent signals.

The spectral width of IS signals increases with altitude and higher PMWE layers also reveal broader spectra (i.e. in terms of turbulent interpretation stronger turbulence); see Fig. 3 and Table 1. In order to consider spectral width as a function of altitude, we separate the distribution shown in Fig. 13 (left panel) in 6 altitude bins (see Fig. 14). Between 60 and 63 km the maximum of the distribution is at $2\,\mathrm{m\,s}^{-1}$. In the highest altitude bin (i.e. above 75 km), the maximum of the distribution lies between 7 and $9\,\mathrm{m\,s}^{-1}$. In the altitude range from 69–72 km, the distribution is very broad and no significant maxima can be defined. Using Eq. (6) and taking buoyancy frequency of $N = 0.02\,\mathrm{s}^{-1}$ we get energy dissipation rate of $\sim 10\,\mathrm{mW\,kg}^{-1}$ for the lower altitude range and up to $\sim 210\,\mathrm{mW\,kg}^{-1}$ for the higher altitude range. For orientation, a HPHW of $\sim 20\,\mathrm{m\,s}^{-1}$ yields an energy dissipation rate of $1\,\mathrm{W\,kg}^{-1}$.

It interesting to note in this context that Kishore Kumar et al. (2007) found a correlation between the occurrence rate of low-latitude mesosphere echoes (which have characteristics reminiscent to those of PMWE) with lower mesospheric inversion layers (MILs) during equinoxes. They pointed out that broad spectra measured with the Indian MST Radar located in Gadanki are associated with so-called lower MILs observed by the co-located Rayleigh lidar and that both are related to strong turbulence activity at those heights. Lidar observations at mid-latitudes by Whiteway et al. (1995); Thomas et al. (1996); Liu et al. (2004) and high-latitudes by Cutler et al. (2001); Duck and Greene (2004); Collins et al. (2011) have shown that MILs are often associated with turbulence activity which is reflected in the lidar temperature measurements as an adiabatic lapse rate on top of the inversion layers. On the other hand, numerical simulations by Liu et al. (2000) showed that vigorous turbulence is required to change the thermal structure to the shape associated with temperature inversions. Also, Thomas et al. (1996) found a connection between MILs observed with Rayleigh lidar and winter radar echoes observed by their VHF radar, and concluded that the reason was strong turbulence activity. We note that our findings are consistent with these observations and suggest that the PMWE are not only associated with turbulence which in turn may be closely connected to mesospheric inversion layers. The latter hypothesis, however, needs further investigation and cannot be verified or falsified based on the EISCAT measurements alone.

7 Summary

In this work we considered two examples of PMWE (weak and strong) measured with the EISCAT VHF radar observed on two consecutive days. The strong PMWE event lasted for a total of 6 h and strong gradients in observed vertical winds were detected. Inside the layer the spectra were broadened. Horizontal winds observed with the SAURA MF radar showed high values of up to $200\,\mathrm{m\,s}^{-1}$ at corresponding altitudes. Neither of these features is reproduced on the other day of the observations, when only weak PMWE was detected. Our study showed that only the parameter n was consistent in all the considered observations. This parameter characterizes the shape of the backscattered signal. For usual IS measurements in the D-region this parameter reveals a value of 1 (Strelnikova and Rapp, 2010; Strelnikova and Rapp, 2011). In case of strong VHF PMSE, this parameter is statistically concentrated around 2. In the case of weak UHF PMSE as well as in the case of VHF PMWE (both cases are characterized by comparable volume reflectivities) this parameter reveals some intermediate value (i.e. $1 < n < 2$) with a broad distribution and a maximum at 1.6.

This unambiguously confirms that some other mechanism (not IS or, at least not IS alone) is responsible for such echoes. This parameter alone cannot shed light on the nature of this phenomenon, but casts doubt on the explanation of PMWE as highly damped ion-acoustic waves with typical D-region spectra (Kirkwood et al., 2006b).

On the other hand, neutral air turbulence alone cannot explain the volume reflectivities measured by the EISCAT VHF radar. In order to explain such volume reflectivities, charged aerosols (most likely meteoric smoke particles) in combination with neutral turbulence are required. Also, in the absence of charged aerosols the estimation of the energy dissipation rate is not possible. The well-known relation, Eg. (6), by Hocking (1985) between spectral width and energy dissipation rate is only valid in the inertial subrange of the turbulence spectrum of the neutral gas. Assuming that the presence of charged aerosols extends the power spectrum of electrons down to smaller scales (smaller than Bragg scale of the EISCAT VHF radar, i.e. 67 cm), the energy dissipation rate can be estimated. We analyzed ~ 32.5 h of the EISCAT VHF PMWE observations and found a broad distribution of energy dissipation rates with a median value of $\sim 240\,\mathrm{mW\,kg^{-1}}$.

The broadening of spectra inside the PMWE layer was computed by means of the ratio of the measured spectral width to a theoretical width assuming pure incoherent scatter. In 91.7 % of all observations this ratio was larger than 1. In 77.3 % this ratio was larger than 1.575, i.e. the median value of this ratio for altitudes of PMWE location. Note that at PMWE altitudes in the absence of PMWE, only 75 % of observations revealed values larger than 1.

The vertical wind observations did not show any prominent features inside the PMWE layers in comparison to surrounding, i.e. non-PMWE media. Only a weak shift of the median values of wind speed and wind gradient was found.

Thus, in this work we summarized all the features of PMWE measured by with the EISCAT VHF radar. Unfortunately, these measurements are not sufficient to unambiguously explain the nature of PMWE. In the future, independent measurements of energy dissipation rates and charged meteoric smoke particles during PMWE events should be conducted and combined with simultaneous and common volume radar observations at various frequencies.

Acknowledgements. EISCAT is an international association supported by the research councils of of Norway, Sweden, Finland, Japan, China, the United Kingdom and Germany.

Topical Editor C. Jacobi thanks M. Rietveld and one anonymous referee for their help in evaluating this paper.

References

Baron, M.: EISCAT progress 1983–1985, J. Atmos. Terr. Phys., 48, 767–772, 1986.

Batchelor, G. K.: Small-scale variation of convected quantities like temperature in turbulent fluid. Part 1. General discussion and the case of small conductivity, J. Fluid Mech., 5, 113–133, 1959.

Belova, E., Kirkwood, S., Ekeberg, J., Osepian, A., Häggström, I., Nilsson, H., and Rietveld, M.: The dynamical background of polar mesosphere winter echoes from simultaneous EISCAT and ESRAD observations, Ann. Geophys., 23, 1239–1247, doi:10.5194/angeo-23-1239-2005, 2005.

Belova, E., Smirnova, M., Rietveld, M. T., Isham, B., Kirkwood, S., and Sergienko, T.: First observation of the overshoot effect for polar mesosphere winter echoes during radiowave electron temperature modulation, Geophys. Res. Lett., 35, L03110, doi:10.1029/2007GL032457, 2008.

Brattli, A., Blix, T. A., Lie-Svendsen, Ø., Hoppe, U.-P., Lübken, F.-J., Rapp, M., Singer, W., Latteck, R., and Friedrich, M.: Rocket measurements of positive ions during polar mesosphere winter echo conditions, Atmos. Chem. Phys., 6, 5515–5524, doi:10.5194/acp-6-5515-2006, 2006.

Cho, J. Y. N., Hall, T. M., and Kelley, M. C.: On the role of charged aerosols in polar mesosphere summer echoes, J. Geophys. Res., 97, 875–886, 1992.

Collis, P. N. and Rietveld, M. T.: Mesospheric observations with the EISCAT UHF radar during polar cap absorption events: 3. Comparison with simultaneous EISCAT VHF measurements, Ann. Geophys., 16, 1355–1366, doi:10.1007/s00585-998-1355-4, 1998.

Collis, P. N., Rietveld, M. T., Rottger, J., and Hocking, W. K.: Turbulence scattering layers in the middle-mesosphere observed by the EISCAT 224-MHz radar, Radio Sci., 27, 97–107, doi:10.1029/91RS02963, 1992.

Collins, R. L., Lehmacher, G. A., Larsen, M. F., and Mizutani, K.: Estimates of vertical eddy diffusivity in the upper mesosphere in the presence of a mesospheric inversion layer, Ann. Geophys., 29, 2019–2029, doi:10.5194/angeo-29-2019-2011, 2011.

Cutler, L. J., Collins, R. L., Mizutani, K., and Itabe, T.: Rayleigh lidar observations of mesospheric inversion layers at Poker Flat, Alaska (65deg N, 147deg W), Geophys. Res. Lett., 28, 1467–1470, doi:10.1029/2000GL012535, 2001.

Czechowsky, P., Ruester, R., and Schmidt, G.: Variations of mesospheric structures in different seasons, Geophys. Res. Lett., 6, 459–462, doi:10.1029/GL006i006p00459, 1979.

Dougherty, J. P. and Farley, D. T.: A theory of incoherent scattering of radio waves by a plasma: 3. Scattering in a partly ionized gas, J. Geophys. Res., 68, 5473–5486, 1963.

Duck, T. J. and Greene, M. D.: High Arctic observations of mesospheric inversion layers, Geophys. Res. Lett., 31, L02105, doi:10.1029/2003GL018481, 2004.

Ecklund, W. L. and Balsley, B. B.: Long-term observations of the Arctic mesosphere with the MST radar at Poker Flat, Alaska, J. Geophys. Res., 86, 7775–7780, doi:10.1029/JA086iA09p07775, 1981.

Hall, C. M., Manson, A. H., Meek, C. E., and Nozawa, S.: Mesospheric turbulence during PMWE-conducive conditions, Atmos. Chem. Phys. Discuss., 7, 7035–7049, doi:10.5194/acpd-7-7035-2007, 2007.

Hansen, G., Hoppe, U.-P., Turunen, E., and Pollari, P.: Comparison of observed and calculated incoherent scatter spectra from the D-region, Radio Sci., 26, 1153–1164, 1991.

Hedin, A. E.: Extension of the MSIS thermosphere model into the middle and lower atmosphere, J. Geophys. Res., 96, 1159–1172, 1991.

Heisenberg, W.: Zur statistischen Theorie der Turbulenz, Z. Physik, 124, 628–657, 1948.

Hill, R. J.: Nonneutral and quasi-neutral diffusion of weakly ionized multiconstituent plasma, J. Geophys. Res., 83, 989–998, 1978.

Hocking, W. K.: Measurement of turbulent energy dissipation rates in the middle atmosphere by radar techniques: A review, Radio Sci., 20, 1403–1422, doi:10.1029/RS020i006p01403, 1985.

Hocking, W. K. and Röttger, J.: Studies of polar mesosphere summer echoes over EISCAT using calibrated signal strengths and statistical parameters, Radio Sci., 32, 1425–1444, doi:10.1029/97RS00716, 1997.

Jackel, B. J.: Characterization of auroral radar power spectra and autocorrelation functions, Radio Sci., 35, 1009–1024, 2000.

Kelley, M. C., Farley, D. T., and Röttger, J.: The effect of cluster ions on anomalous VHF backscatter from the summer polar mesosphere, Geophys. Res. Lett., 14, 1031–1034, 1987.

Kero, A., Enell, C.-F., Kavanagh, A. J., Vierinen, J., Virtanen, I., and Turunen, E.: Could negative ion production explain the polar mesosphere winter echo (PMWE) modulation in active HF heating experiments?, Geophys. Res. Lett., 35, L23102, doi:10.1029/2008GL035798, 2008.

Kirkwood, S.: Polar Mesosphere WINTER Echoes – A review of recent results, Adv. Space Res., 40, 751–757, doi:10.1016/j.asr.2007.01.024, 2007.

Kirkwood, S., Barabash, V., Belova, E., Nilsson, H., Rao, N., Stebel, K., Osepian, A., and Chilson, P. B.: Polar mesosphere winter echoes during solar proton events, Adv. Pol. Up. Atmos. Res., 16, 111–125, 2002.

Kirkwood, S., Belova, E., Blum, U., Croskey, C., Dalin, P., Fricke, K.-H., Goldberg, R. A., Manninen, J., Mitchell, J. D., and Schmidlin, F.: Polar mesosphere winter echoes during MaCWAVE, Ann. Geophys., 24, 1245–1255, doi:10.5194/angeo-24-1245-2006, 2006a.

Kirkwood, S., Chilson, P., Belova, E., Dalin, P., Häggström, I., Rietveld, M., and Singer, W.: Infrasound – the cause of strong Polar Mesosphere Winter Echoes?, Ann. Geophys., 24, 475–491, doi:10.5194/angeo-24-475-2006, 2006b.

Kishore Kumar, G., Venkat Ratnam, M., Patra, A. K., Jagannadha Rao, V. V. M., Vijaya Bhaskara Rao, S., and Narayana Rao, D.: Climatology of low-latitude mesospheric echo characteristics observed by Indian mesosphere, stratosphere, and troposphere radar, J. Geophys. Res., 112, D06109, doi:10.1029/2006JD007609, 2007.

Kolmogoroff, A.: The local structure of turbulence in incompressible viscous fluid for very large Reynolds' numbers, Dokl. Akad. Nauk SSSR, 30, 301–305, 1941.

La Hoz, C. and Havnes, O.: Artificial modification of polar mesospheric winter echoes with an RF heater: Do charged dust particles play an active role?, J. Geophys. Res., 113, D19205, doi:10.1029/2008JD010460, 2008.

La Hoz, C., Havnes, O., Naesheim, L. I., and Hysell, D. L.: Observations and theories of polar mesospheric summer echoes at a Bragg wavelebgth of 16 cm, J. Geophys. Res., 111, D04203, doi:10.1029/2005JD006044, 2006.

Li, Q., Rapp, M., Röttger, J., Latteck, R., Zecha, M., Strelnikova, I., Baumgarten, G., Hervig, M., and Hall, C.: Microphysical parameters of mesospheric ice clouds derived from calibrated observations of polar mesosphere summer echoes at Bragg wavelengths of 2.8 m and 30 cm, J. Geophys. Res., 115, D00I13, doi:10.1029/2009JD012271, 2010.

Liu, A. Z., Roble, R. G., Hecht, J. H., Larsen, M. F., and Gardner, C. S.: Unstable layers in the mesopause region observed with na lidar during the turbulent oxygen mixing experiment (tomex) campaign, J. Geophys. Res., 109, D02S02, doi:10.1029/2002JD003056, 2004.

Liu, H.-L., Hagan, M. E., and Roble, R. G.: Local mean state changes due to gravity wave breaking modulated by the diurnal tide, J. Geophys. Res., 105, 12381–12396, doi:10.1029/1999JD901163, 2000.

Lübken, F.-J.: Seasonal variation of turbulent energy dissipation rates at high latitudes as determined by in situ measurements of neutral density fluctuations, J. Geophys. Res., 102, 13441–13456, doi:10.1029/97JD00853, 1997a.

Lübken, F.-J.: Seasonal variation of turbulent energy dissipation rates at high latitudes as determined by insitu measurements of neutral density fluctuations, J. Geophys. Res., 104, 13441–13456, 1997b.

Lübken, F., Hillert, W., Lehmacher, G., and von Zahn, U.: Experiments revealing small impact of turbulence on the energy budget of the mesosphere and lower thermosphere, J. Geophys. Res., 98, 20369–20384, 1993a.

Lübken, F.-J., Hillert, W., Lehmacher, G., and von Zahn, U.: Experiments revealing small impact of turbulence on the energy budget of the mesosphere and lower thermosphere, J. Geophys. Res., 98, 20369–20384, doi:10.1029/93JD02055, 1993b.

Lübken, F.-J., Strelnikov, B., Rapp, M., Singer, W., Latteck, R., Brattli, A., Hoppe, U.-P., and Friedrich, M.: The thermal and dynamical state of the atmosphere during polar mesosphere winter echoes, Atmos. Chem. Phys., 6, 13–24, doi:10.5194/acp-6-13-2006, 2006.

Lübken, F.-J., Singer, W., Latteck, R., and Strelnikova, I.: Radar measurements of turbulence, electron densities, and absolute reflectivities during polar mesosphere winter echoes (PMWE), Adv. Space Res., 40, 758–764, doi:10.1016/j.asr.2007.01.015, 2007.

Mathews, J. D.: The effect of negative ions on collision-dominated Thomson scattering, J. Geophys. Res., 83, 505–512, 1978.

Mathews, J. D.: The incoherent scatter radar as a tool for studying the ionospheric D-region, J. Atmos. Terr. Phys., 46, 975–986, 1984.

Megner, L., Siskind, D. E., Rapp, M., and Gumbel, J.: Global and temporal distribution of meteoric smoke: A two-dimensional study, J. Geophys. Res., 113, D03202, doi:10.1029/2007JD009054, 2008.

Moorcroft, D. R.: The shape of auroral backscatter spectra, Geophys. Res. Lett., 31, 9802, doi:10.1029/2003GL019340, 2004.

Morris, R. J., Klekociuk, A. R., and Holdsworth, D. A.: First observations of southern hemisphere polar mesosphere winter echoes including conjugate occurrences at $\sim 69^\circ$ S latitude, Geophys. Res. Lett., 38, L03811, doi:10.1029/2010GL046298, 2011.

Raizada, S., Sulzer, M. P., Tepley, C. A., Gonzalez, S. A., and Nicolls, M. J.: Inferring D region parameters using improved in-

coherent scatter radar techniques at Arecibo, J. Geophys. Res., 113, A12302, doi:10.1029/2007JA012882, 2008.

Rapp, M. and Lübken, F.-J.: On the nature of PMSE: Electron diffusion in the vicinity of charged particles revisited, J. Geophys. Res., 108, 8437, doi:10.1029/2002JD002857, 2003.

Rapp, M. and Lübken, F.-J.: Polar mesosphere summer echoes (PMSE): Review of observations and current understanding, Atmos. Chem. Phys., 4, 2601–2633, doi:10.5194/acp-4-2601-2004, 2004.

Rapp, M., Strelnikova, I., and Gumbel, J.: Meteoric smoke particles: Evidence from rocket and radar techniques, Adv. Space Res., 40, 809–817, doi:10.1016/j.asr.2006.11.021, 2007.

Rapp, M., Strelnikova, I., Latteck, R., Hoffmann, P., Hoppe, U., Haggstrom, I., and Rietveld, M.: Polar mesosphere summer echoes (PMSE) studied at Bragg wavelengths of 2.8 m, 67 cm, and 16 cm, J. Atmos. Sol. Terr. Phys., 70, 947–961, doi:10.1016/j.jastp.2007.11.005, 2008.

Rapp, M., Latteck, R., Stober, G., Hoffmann, P., Singer, W., and Zecha, M.: First three-dimensional observations of polar mesosphere winter echoes: Resolving space-time ambiguity, J. Geophys. Res., 116, A11307, doi:10.1029/2011JA016858, 2011.

Rietveld, M. T. and Collis, P. N.: Mesospheric observations with the EISCAT UHF radar during polar cap absorption events: 2. Spectral measurements, Ann. Geophys., 11, 797–808, 1993.

Röttger, J. and La Hoz, C.: Characteristics of polar mesosphere summer echoes (PMSE) observed with the EISCAT 224 MHz radar and possible explanations of their origin, J. Atmos. Terr. Phys., 52, 893–906, 1990.

Röttger, J., Rietveld, M. T., LaHoz, C., Hall, C., Kelley, M. C., and Swartz, W.: Polar mesosphere summer echoes observed with the EISCAT 933-MHz radar and the CUPRI 46.9 MHz radar, their similarity to 224 MHz radar echoes and their relation to turbulence and electron density profiles, Radio Sci., 25, 671–687, 1990.

Singer, W., Keuer, D., and Eriksen, W.: The ALOMAR MF radar: Technical design and first results, in: Proceedings of the 13th ESA Symposium on European Rocket and Balloon Programmes and Related Research, Oeland, Sweden (ESA SP–397), vol. ESA SP-397, edited by: Kaldeich-Schürmann, B., pp. 101–104, 1997.

Singer, W., Latteck, R., Holdsworth, D. A., and Kristiansen, T.: A new narrow beam MF radar at 3 MHz for studies of the high-latitude middle atmosphere: System description and first results, Proceedings of MST10, 13–20 May 2003, Piura, Peru, pp. 385–390, 2003.

Singer, W., Latteck, R., and Holdsworth, D. A.: A new narrow beam Doppler radar at 3 MHz for studies of the high-latitude middle atmosphere, Adv. Space Res., 41, 1487–1493, doi:10.1016/j.asr.2007.10.006, 2007.

Stebel, K., Blum, U., Fricke, K. H., Kirkwood, S., Mitchell, N. J., and Osepian, A.: Joint radar/lidar observations of possible aerosol layers in the winter mesosphere, J. Atmos. Sol. Terr. Phys., 66, 957–970, doi:10.1016/j.jastp.2004.03.008, 2004.

Strelnikova, I. and Rapp, M.: Studies of polar mesosphere summer echoes with the EISCAT VHF and UHF radars: Information contained in the spectral shape, Adv. Space Res., 45, 247–259, doi:10.1016/j.asr.2009.09.007, 2010.

Strelnikova, I. and Rapp, M.: Majority of PMSE spectral widths at UHF and VHF are compatible with a single scattering mechanism, J. Atmos. Sol. Terr. Phys., pp. 2142–2152, doi:10.1016/j.jastp.2010.11.025, 2011.

Thomas, L., Marsh, A. K. P., Wareing, D. P., Astin, I., and Chandra, H.: VHF echoes from the midlatitude mesosphere and the thermal structure observed by lidar, J. Geophys. Res., 101, 12867–12878, doi:10.1029/96JD00218, 1996.

Varney, R. H., Kelley, M. C., Nicolls, M. J., Heinselman, C. J., and Collins, R. L.: The electron density dependence of polar mesospheric summer echoes, J. Atmos. Sol. Terr. Phys., 73, 2153–2165, doi:10.1016/j.jastp.2010.07.020, 2011.

Whiteway, J. A., Carswell, A. I., and Ward, W. E.: Mesospheric temperature inversions with overlying nearly adiabatic lapse rate: An indication of a well-mixed turbulent layer, Geophys. Res. Lett., 22, 1201–1204, doi:10.1029/95GL01109, 1995.

Zeller, O., Zecha, M., Bremer, J., Latteck, R., and Singer, W.: Mean characteristics of mesosphere winter echoes at mid- and high-latitudes, J. Atmos. Sol. Terr. Phys., 68, 1087–1104, doi:10.1016/j.jastp.2006.02.015, 2006.